Validation of reinforced concrete pile caps using non-linear finite element analysis and finite element limit analysis

Andersen, M.E.M.; Jensen, T.W.; Poulsen, P.N.; Olesen, J.F.; Hoang, L.C.

Published in:
Computational Modelling of Concrete and Concrete Structures

Link to article, DOI:
10.1201/9781003316404-37

Publication date:
2022

Document Version
Publisher's PDF, also known as Version of record

Computational Modelling of Concrete and Concrete Structures – Meschke, Pichler & Rots (Eds)

Validation of reinforced concrete pile caps using non-linear finite element analysis and finite element limit analysis

M.E.M. Andersen & T.W. Jensen
Department of Bridges International, COWI A/S, Kongens Lyngby, Denmark

P.N. Poulsen, J.F. Olesen & L.C. Hoang
Department of Civil Engineering, The Technical University of Denmark, Kongens Lyngby, Denmark

ABSTRACT: Analysis methods based on the rigid-plastic material models, such as the strut-and-tie method (STM), are often used to validate the designs of solid reinforced concrete structures in the ultimate limit state. However, the validation can be quite cumbersome since it involves much manual labor. Another analysis method based on the rigid-plastic material model is Finite Element Limit Analysis (FELA). The workflow when using FELA is easily automatized since the method is fully numerical. The capacity, stress fields, and collapse mode of the structure are the results that can be obtained from a FELA analysis. Another fully numerical method for validating solid reinforced concrete structures is the Non-Linear Finite Element Method (NLFEM). Using advanced material models, NLFEM programs such as DIANA FEA can accurately describe the structural behavior of reinforced concrete structures, even post the peak load. However, this modeling precision comes at the cost of increased complexity, and many material parameters are required for the models. This trade-off between precision and complexity in NLFEM is in contrast to FELA, which requires very few material parameters but only provides information about the structure at peak load. In this paper, the two methods are briefly introduced, whereafter they are compared by analyzing two four-pile cap experiments. Results obtained from the two models are presented and compared both to each other and to the experimental results. At the end, conclusions about the strengths and weaknesses of the two types of analysis are drawn.

1 INTRODUCTION

Design and validation of pile caps for the ultimate limit state are often performed using the Strut-and-Tie Method (STM). This method is based on the lower bound theorem for rigid-plastic materials and thus provides safe designs. However, STM can be inefficient to use, especially when many load cases and different geometries need to be considered. Numerical rigid-plastic limit analysis can be performed using Finite Element Limit Analysis (FELA) (Anderheggen & Knöpfel 1972). The method utilizes a rigid-plastic material model and is, similarly to STM, based on the extremum principles for rigid-plastic materials (Drucker, Prager, & Greenberg 1952; Gvozdev 1960). FELA has been known since the seventies and has been used for geotechnical calculations for several years. Recently, FELA has become popular in reinforced concrete design and has been applied to slab structures (Jensen, Poulsen, & Hoang 2018), wall structures (Poulsen & Damkilde 2000; Herfelt 2017), and solid structures (Vincent, Arquier, Bleyer, & de Buhan 2018; Vincent, Arquier, Bleyer, & de Buhan 2020; Andersen, Poulsen, & Olesen 2021). FELA has reached a mature state for plane reinforced concrete structures, and the first commercial programs are now in use to design and evaluate these structures (Herfelt, Krabbenhøft, & Krabbenhøft 2019).

A requirement for the use of FELA is that the structure should have sufficient deformation capability to enable redistributing of stresses and the development of the predicted collapse mechanism. That is, the structures should exhibit a sufficiently ductile behavior. Ductility is normally achieved by ensuring that yielding of the reinforcement is governing for the capacity, rather than crushing of concrete or rupture of reinforcement. Plane structures that are designed using codes and guidelines possess this ductility provided by minimum reinforcement. For solid reinforced concrete structures, which often do not have minimum reinforcement, the presence of sufficient ductility is not always guaranteed. The presence of the required ductility can be shown by full-scale testing. However, this is not feasible in practice. Instead, advanced non-linear finite element (NLFEM) calculations can be performed, giving a more realistic prediction of the behavior of the structure before the collapse.

This paper studies a series of experiments of reinforced concrete four-pile caps subjected to central

 DOI 10.1201/9781003316404-37

compressive loading (Miguel-Tortola, Miguel, & Pallarés 2019). The pile caps are analyzed using FELA and NLFEM. In the FELA model, constant stress elements with normal traction continuity on inter-element surfaces and shear equilibrium in the nodes are used (Andersen, Poulsen, & Olesen 2022). The Modified Mohr-Coulomb yield criterion is used for the concrete with a possible inclusion of the effectiveness factor on the concrete compressive strength and with the inclusion of smeared reinforcement. The NLFEM is modeled in DIANA FEA (DIANA 2017), where a smeared cracking approach is used for concrete in tension, and lateral cracking is considered for reduction of the concrete compressive strength. The material parameters for FELA and NLFEM are based on model codes and guidelines for an objective comparison. The results obtained using the two numerical methods are compared to experimental results, and conclusions are drawn concerning the usefulness of FELA compared to NLFEM for analysis of pile caps.

2 FINITE ELEMENT LIMIT ANALYSIS

Finite Element Limit Analysis (FELA) combines the domain discretization of the finite element method with limit analysis based on a rigid-plastic material model. FELA was first suggested by Anderheggen & Knöpfel (1972) for reinforced concrete membranes and plates and are now used to analyze both geotechnical and reinforced concrete structures in the ultimate limit state.

Limit analysis with a rigid-plastic material model was developed independently by Gvozdev (1960) and Drucker, Prager, & Greenberg (1952) who formulated the extremum principles of rigid-plastic materials. These extremum principles are the lower bound theorem, the upper bound theorem, and the uniqueness theorem. For a thorough review, see (Nielsen & Hoang 2011).

FELA can be based on either the lower bound theorem where a statically admissible stress state is sought or on the upper bound theorem where a kinematically admissible collapse mode is sought. The method used in this paper is based on the lower bound theorem but in a relaxed manner. Consequently, a lower bound on the failure load is not guaranteed. However, the solution will still converge towards the failure load.

In FELA, the structure is divided into several stress-based finite elements. The element which is used is the Normal Traction element (Andersen, Poulsen, & Olesen 2022), which is a partially mixed lower bound element. The element has a constant stress field and thus only one stress point per element. Each stress point corresponds to a full triaxial stress state:

$$\boldsymbol{\sigma}^\top = \begin{bmatrix} \sigma_{xx} & \sigma_{yy} & \sigma_{zz} & \sigma_{xy} & \sigma_{xz} & \sigma_{zy} \end{bmatrix} \tag{1}$$

The stress state of the element needs to be in equilibrium with that of neighboring elements through the force equilibrium of corner nodes and traction equilibrium of the faces.

The shear stress contributions are placed in the corner nodes. The equilibrium for a single node is given by:

$$\sum_{i=1}^{m} Q_{i,n}(\boldsymbol{\sigma}_i) = P_n \tag{2}$$

where $Q_{i,n}$ is the force contribution in the node from element i, which is a function of the stress state of element i, and P_n is the external loading of the node. The subscript n, denotes either the x, y, or z direction. Similarly, the traction equilibrium for an interface between two elements is given by:

$$t_{1,n}(\boldsymbol{\sigma}_1) + t_{2,n}(\boldsymbol{\sigma}_2) = q_n \tag{3}$$

where $t_{1,n}$ and $t_{2,n}$ is the traction for the elements on either side of the interface, and q_n is a traction load on the interface. Here the subscript n denotes the normal direction on the interface since the element only considers strict traction continuity for the normal traction.

The stress point vectors are collected into the system stress vector, $\boldsymbol{\beta}^\top = \begin{bmatrix} \boldsymbol{\sigma}_1^\top & \dots & \boldsymbol{\sigma}_n^\top \end{bmatrix}$. The stress continuity between the elements and the elements and the loading is ensured via the equilibrium matrix $\mathbf{H}$, which has contributions from each of the elements. The equilibrium matrix, $\mathbf{H}$, multiplied with the system stress vector, $\boldsymbol{\beta}$, should be in equilibrium with the constant loads $\mathbf{R}_0$ and scalable loads $\mathbf{R}\lambda$, where λ is the so-called load-factor, which is sought to be maximized. Furthermore, the stress state in each element should abide by the employed yield criteria. Combined, this gives an optimization problem on the form:

$$\begin{aligned} &\text{max.} && \lambda && \text{Load} && (4a)\\ &\text{s.t.} && \mathbf{H}\boldsymbol{\beta} = \mathbf{R}_0 + \lambda\mathbf{R} && \text{Stress equilibrium} && (4b)\\ & && f_i(\boldsymbol{\sigma}_i) \le 0 && \text{Yield conditions} && (4c) \end{aligned}$$

The optimization problem above is convex and can to be efficiently solved when certain criteria are met. For the present case the yield conditions (4c) are modeled as semidefinte constraints, and these coupled with an affine objective function (4a) and affine equality constraints (4b) are indeed convex (Boyd & Vandenberghe 2004).

In the following the basis of the stress equilibrium (4a) and the yield conditions (4c) will be briefly elaborated. However, for a thorough examination of the model see Andersen, Poulsen, & Olesen (2022).

2.1 Stress equilibrium

The element used for the FELA analysis of this paper is the Normal Traction element. A sketch of the element can be seen in Figure 1. The element is a so-called partially mixed lower bound element. *Partially* mixed

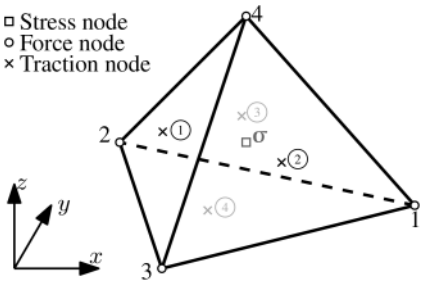

Figure 1. Configuration of the Normal Traction element (Andersen, Poulsen, & Olesen 2022).

because it has strict normal traction continuity on the element faces, but only a relaxed shear traction continuity moved unto the corner nodes as a force equilibrium.

The element contains only one stress node and consequently only one material point, which means that each element has a computational requirement of only one-third of a regular linear stress element. This reduced computational cost per element is desirable when large solid geometries must be modeled, requiring many elements to mesh adequately. Furthermore, the element has proved to have fast convergence (Andersen, Poulsen, & Olesen 2022).

2.2 Reinforced concrete yield condition

The stress state of each element needs to abide by a yield condition. In this paper, a yield condition for reinforced concrete based on a separation of stresses into concrete stresses and reinforcement stresses is utilized (here shown as tensors):

$$\boldsymbol{\sigma}_{\square} = \boldsymbol{\sigma}_{\square,c} + \boldsymbol{\rho}\boldsymbol{\sigma}_{\square,s} \tag{5}$$

where $\boldsymbol{\sigma}_{\square}$ is the total stress tensor, $\boldsymbol{\sigma}_{\square,c}$ is the concrete stress tensor given by:

$$\boldsymbol{\sigma}_{\square,c} = \begin{bmatrix} \sigma_{c,xx} & \sigma_{c,xy} & \sigma_{c,xz} \\ \sigma_{c,xy} & \sigma_{c,yy} & \sigma_{c,zy} \\ \sigma_{c,xz} & \sigma_{c,zy} & \sigma_{c,zz} \end{bmatrix} \tag{6}$$

and $\boldsymbol{\rho}\boldsymbol{\sigma}_{\square,s}$ is the smeared reinforcement stress tensor given by:

$$\boldsymbol{\rho}\boldsymbol{\sigma}_{\square,s} = \begin{bmatrix} \rho_x & 0 & 0 \\ 0 & \rho_y & 0 \\ 0 & 0 & \rho_z \end{bmatrix} \begin{bmatrix} \sigma_{s,xx} & 0 & 0 \\ 0 & \sigma_{s,yy} & 0 \\ 0 & 0 & \sigma_{s,zz} \end{bmatrix} \tag{7}$$

where $\boldsymbol{\rho}$ contains the reinforcement degree in each of the three normal directions, and $\boldsymbol{\sigma}_{\square,s}$ is the stress in the reinforcement. As can be seen this assumes that the reinforcement is placed in accordance with the *xyz*-coordinate system, and that only normal stresses can be carried by the reinforcement. This separation of stresses is analogue to the way the Nielsen yield criterion is developed (Nielsen & Hoang 2011).

2.2.1 Concrete yield criterion

For the concrete stresses the Modified Mohr-Coulomb yield criterion is used. The yield criterion consist of a friction and a separation criterion and are cast in principal stresses:

$$\sigma_1 \leq \nu_t f_t \tag{8a}$$
$$k\sigma_1 - \sigma_3 \leq \nu f_c \tag{8b}$$

here σ_1 and σ_3 is the largest and smallest principal stress respectively, k is the friction coefficient usually taken as 4, and $\nu_t f_t$ and νf_c are the effective tensile and compressive strength, respectively.

The effective tensile strength is chosen as a small fraction of the effective compressive strength, $\nu_t f_t = \nu f_c / C \approx 0$, where C is a number larger than 1000. The small value of the tensile strength has a negligible influence on the capacity, but improves the quality of the dual variables of the equilibrium equations (4b). The dual variables can be interpreted as the collapse mechanism of the structure (Poulsen & Damkilde 2000).

The conditions of (8a) and (8b) can be cast as a set of two semidefinite constraints with two additional linear constrains and auxiliary variables (Larsen 2010; Martin & Makrodimopoulos 2008; Krabbenhøft, Lyamin, & Sloan 2008; Bisbos & Pardalos 2007):

$$\begin{aligned} \boldsymbol{\sigma}_{\square,c} + (k\alpha_1)\mathbf{I} &\preceq 0 \\ \boldsymbol{\sigma}_{\square,c} - \alpha_2\mathbf{I} &\succeq 0 \\ \alpha_2 &\leq \nu_t f_t \\ \alpha_1 + \alpha_2 &\leq \nu f_c / k \end{aligned} \tag{9}$$

where $\mathbf{I}$ is the identity matrix of order 3, α_1 and α_2 are auxiliary variables, and the symbols $\succeq 0$ and $\preceq 0$ designate positive and negative semi-definiteness, respectively.

2.2.2 Reinforcement yield conditions

The reinforcement stresses are constrained using a set of simple linear constraints on the form:

$$-f_{s,c} \leq \sigma_{s,xx} \leq f_s \tag{10a}$$
$$-f_{s,c} \leq \sigma_{s,yy} \leq f_s \tag{10b}$$
$$-f_{s,c} \leq \sigma_{s,zz} \leq f_s \tag{10c}$$

where $f_{s,c}$ is the reinforcement compressive yield strength, which is set to 0, and f_s is the reinforcement tensile yield strength.

3 NON-LINEAR FINITE ELEMENT ANALYSIS

The commercial program DIANA FEA (DIANA 2017) is used to perform the analysis.

The total strain crack model in DIANA FEA is used, which is based on the modified compression theory

(Vecchio & Collins 1986). The reinforcement bars are modeled with embedded truss elements with bond slip.

The concrete in the model is discretized with solid hexahedron elements with 20 nodes and a quadratic displacement interpolation. The average side length of the element is 50 mm. The reinforcement bars are modeled with embedded truss elements and connected to the solid elements with line interface elements to enable modeling of the bond-slip between the reinforcement and the concrete.

The equilibrium between the external and internal forces is achieved iteratively with the Newton-Raphson method and line-search. For the convergence criterion, the energy norm is chosen with a tolerance of 0.001. The step sizes used in the analyses are between 0:25 mm and 1:00 mm.

3.1 Material models

The following material models are used in the NLFEA.

Concrete

The material parameters not presented in the following sections are calculated with the equations stated in fib model code 2010 (Fib 2013), and the guidelines from the Dutch Rijkwaterstaat (Hendriks, de Boer, & Belletti 2017).

The *Total Strain Crack Model* in DIANA FEA is used, which is based on the modified compression theory (Vecchio & Collins 1986). The implementation in 3D is according to Selby (1993). The post-peak tensile behavior is modeled as exponential softening with a crack band based on the individual element size. The damage due to cracking reduces the Poissons ratio at the same pace as the reduction of the secant modulus (see (DIANA 2017)).

The compression behavior is modeled with a parabolic stress-strain relation (Feenstra 1993). The relation is based on Young modulus E_c, the compressive strength f_c, the compressive fracture energy G_c, and the crushing bandwidth h_c (which is equivalent to the crack bandwidth). The compressive fracture energy G_c determine the ductility for the concrete. The guidelines (Hendriks, de Boer, & Belletti 2017) recommend $G_c = 250G_f$, where G_f is the tensile fracture energy. However, this value is based on experiments with concrete strength up to 50 MPa (Nakamura & Higai 2001) and is considerately higher than reported elsewhere (Vonk 1992; Lertsrisakulrat, Watanabe, Matsuo, & Niwa 2001). In (Vonk 1992), the compressive fracture energy is reported as $50G_f - 100G_f$. The influence of the compressive fracture energy on the compressive softening behavior is shown in figure 2. The figure shows that the stress-strain relationship for compressive fracture energy of $50G_f$ results in a significantly more brittle failure when compared to $250G_f$. However, to be consistent with the guidelines, initial compressive fracture energy of $250G_f$ is chosen.

The reduction of the compressive strength due to lateral cracking is considered with model B described in (Vecchio & Collins 1993), as shown in Equation (11).

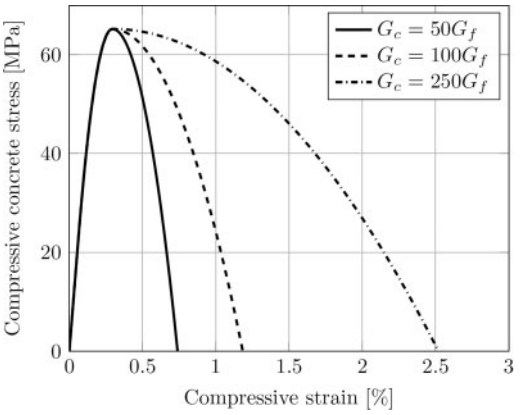

Figure 2. Stress-strain for concrete in compression

In FELA, this effect is taken into account by the effectiveness factor.

$$\beta_{\sigma_{cr}} = \frac{1}{1 + 0.27\left(-\frac{\alpha_{lat}}{\varepsilon_0} - 0.37\right)} \leq 1 \qquad (11)$$

where $\alpha_{lat} = \sqrt{\alpha_{l,1}^2 + \alpha_{l,2}^2}$ and $\alpha_{l,1}$ and $\alpha_{l,2}$ are the lateral strains.

Reinforcement

The reinforcement steel is modeled with Von Mises plasticity and a bilinear plastic strain-stress relation for hardning. The simple stress-strain relationship is estimated to have a minor effect on the behaviour.

The bond between the reinforcement and the concrete is modeled with interface elements. The bond-slip material model from fib model code 2010 (Fib 2013) is used where "good bond condition" and pull-out failure are assumed.

4 FOUR-PILE CAP COMPARISON

4.1 Presentation of specimens

The two methods are used to analyze some specimens of four-pile caps from an experimental campaign by Miguel-Tortola, Miguel, & Pallarés (2019). The experimental campaign consisted of 21 square four-pile caps with slab width of 1.15 m, height varying from 0:25 m to 0:45 m, varying reinforcement layout, and varying loading setup.

In this paper specimens 4P-N-C2 and 4P-N-C3 are considered. These specimens are loaded by a central normal force and have a height of 0.45 m. The geometry of the four-pile cap can be seen in Figure 3. Both have mesh reinforcement at the bottom face. However, only specimen 4P-N-C3 has shear reinforcement. The reinforcement layouts can be seen in Figure 4. The mesh reinforcement had hooked ends to ensure proper anchorage, which the figure does not show. The number of bars can be seen in Table 1, where A_{sB} is the

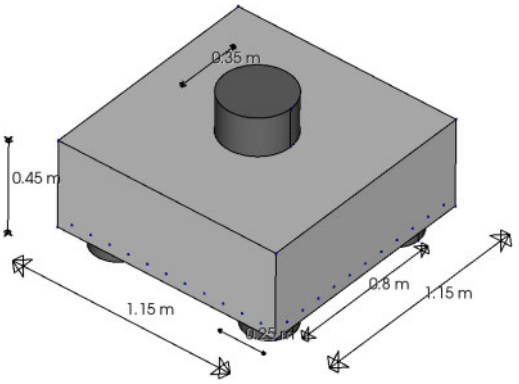

Figure 3. Geometry of the four-pile cap specimens.

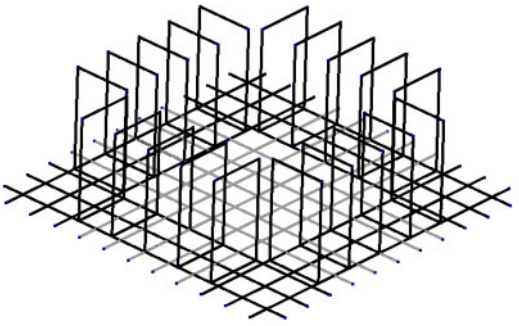

Figure 4. Reinforcement layout of the specimens.

bunched bars over the piles, A_{sH} is the bars between the piles, and A_{sV} is the shear reinforcement. The yield and ultimate strength of the individual bars can be seen in Table 2.

In the experimental setup, the column was fixed, while the load was applied by actuators in each pile to ensure uniform distribution of pile reactions. One actuator was deformation controlled, and the remaining three were synchronized with this and load controlled. The load on the piles was applied through a hinge capable of both rotation and in-plane translation, meaning that only vertical load was applied to the piles.

Table 1 also contains the experimental results of the two specimens with $V_{y,e}$ being the load corresponding to yielding of the bunched reinforcement A_{sB}, $V_{u,e}$ being the ultimate load, and u_z being the vertical deformation at peak load.

Table 2. Material parameters of the reinforcement used in the experiments.

Ø [*mm*]	f_y [*MPa*]	f_u [*MPa*]
8	573.3	650.9
10	519.3	634.7
12	553.8	641.8

4.2 Description of FELA model

The FELA calculations are performed using the COWI software package *fela* programmed in Python. The software package uses GMSH as a mesher and Mosek as a solver. The size of the elements in the model can be adjusted by the so-called characteristic length l_c of the elements. The characteristic length is the side-length of the tetrahedral elements, which the mesher aims at providing.

The reinforcement is modeled as smeared reinforcement, as described earlier. The smeared reinforcement approach means that some choices have to be made regarding how detailed the model needs to be. The most detailed model would be to smear out every reinforcement rod independently. However, this creates a model with numerous overlapping solid regions, which would be complicated both to model and mesh. A less detailed way is to separate the reinforcement into groups and model each group as separate smear regions. The less detailed way is often the most practical solution and can adequately capture the effect of the reinforcement in the model. In this paper, the latter method is used. The reinforcement at the bottom face is separated into two groups; the main bending reinforcement over the piles is in one group, and the reinforcement between the piles in another. The reinforcement groups are then further separated for reinforcement in the x- and y- directions, respectively. The stirrups are separated such that each leg of the stirrup, the bottom, and the top part belong to separate groups. The thickness of the smear regions for the bending reinforcement is set to 50 mm, and the thickness of the shear reinforcement regions is set to 25 mm. Figure 5 shows the smeared reinforcement regions of the model for a mesh with $l_c = 50\ mm$.

4.2.1 Convergence study

A convergence study is made to make sure that the capacity from the calculations is sufficiently

Table 1. Results from the testing of the two specimens (Miguel-Tortola, Miguel, & Pallarés 2019). * Punching after yielding of bunched reinforcement.

Specimen	f_c [*MPa*]	f_t [*MPa*]	A_{sB}	A_{sH}	A_{sV}	$V_{y,e}$ [*kN*]	$V_{u,e}$ [*kN*]	u_z [*mm*]	Failure mode
4P-N-C2	36.3	2.8	$4 \times (2Ø10 + 1Ø12)$	$2 \times 5Ø8$		960.4	1173.9	5.7	Punching*
4P-N-C3	34.0	2.7	$4 \times (2Ø10 + 1Ø12)$	$2 \times 5Ø8$	$4 \times 5Ø8$	1014.1	1317.3	9.7	Flexural

converged. Five computations with characteristic lengths varying between 100 mm and 25 mm is performed. For the convergence study, an effectiveness factor of $\nu = 1.0$ is used. The result of the convergence study can be seen in Figure 6. The solution is converged from the third data point, but the solution precision is adequate from even the first data point. The middle data point of the figure is with a characteristic length of $l_c = 50$ *mm* and has 48610 elements. This mesh is used for the rest of the calculations in this paper.

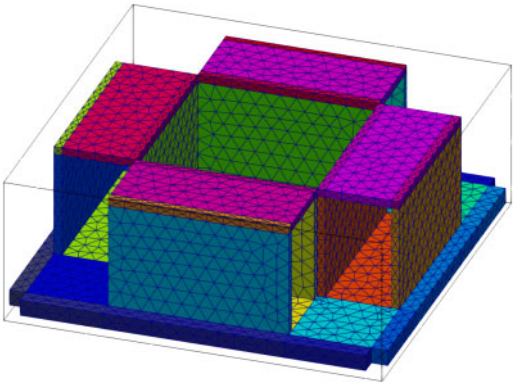

Figure 5. Smeared reinforcement regions for a mesh with characteristic length $l_c = 50$ mm.

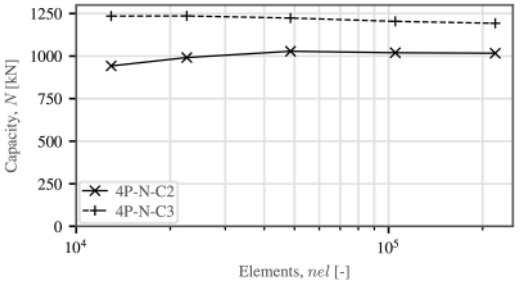

Figure 6. Convergence study for the FELA model.

4.2.2 *Influence of effectiveness factor*

The influence of the effectiveness factor on the capacity is studied by varying the effectiveness factor between 0.2 and 1.0. A plot of the capacity of the two models as a function of the effectiveness factor can be seen in Figure 7. Interestingly, the effectiveness factor does not significantly influence the capacity unless a very low value below 0.4 is used, which is seldom the case for this type of structure.

This observation indicates that the capacity is mainly limited by yielding of the reinforcement, which would indicate that the failures should be flexural or governed by yielding. This is supported by the failure modes from the experiments, which both had yielding of the primary bending reinforcement before failure (Miguel-Tortola, Miguel, & Pallarés 2019). Consequently, an effectiveness factor of $\nu = 1.0$ is used for the FELA calculations in the remainder of this paper.

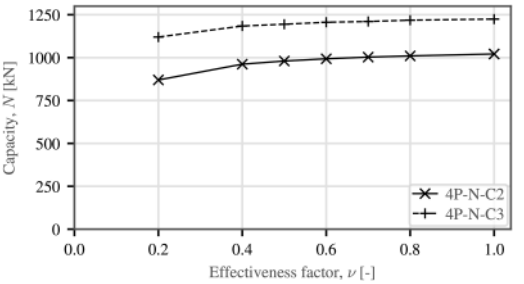

Figure 7. Influence of the effectiveness factor ν on the capacity.

4.3 *Description of DIANA model*

The material properties, not given in Table 1 and Table 2, are based on (Fib 2013) and the guidelines from the Dutch Rijkwaterstaat (Hendriks, de Boer, & Belletti 2017) to ensure an objective comparison. In Table 2, only f_y and f_u are given as material properties for the reinforcement. Thus, a post-yielding stiffness of $0.01E_s$ is chosen to account for the hardening. After the ultimate capacity, f_u, is reached the stiffness is reduced to zero. The model consist of elements with a size of 0.05 m. To get the post peak, deformation controlled load is applied. The load and support are applied on a load-plate, as shown in Figure 3, which is connected to the concrete in the pile cap with an soft interface.

In the following the results from the two different methods are presented, compared, and discussed. First a comparison of the capacity predicted from the two models are performed, as well as the load displacement plot for the DIANA FEA calculations and the experiments. Thereafter the stress flow from the two models are studied. Finally the predicted collapse from the two models are discussed.

4.4 *Results*

4.4.1 *Capacity and load-deflection*

Figure 8 shows the load-displacement plot of the two specimens as well as the same predicted from the DIANA FEA calculations. The capacity found from the FELA calculations is also indicated. The plot shows that the ductility of the two specimens varies quite significantly, with the maximum deflection of the 4P-N-C3 specimen being almost twice that of the 4P-N-C2 specimen. The NLFEA show a more stiff initial behavior compared with the experiments. The material stiffness from the experiments was not measured, so the relation between f_c and E_c was used, which is not an accurate relation. Furthermore, the deformation for the NFLEA is the difference between the top-centre and the point above the supports. After the linear part, both results from the NLFEA shows a decrease of the load. The decrease might be due to the relative low amount of reinforcement which result in small difference between the theoretical uncracked capacity and cracked capacity of the pilecap.

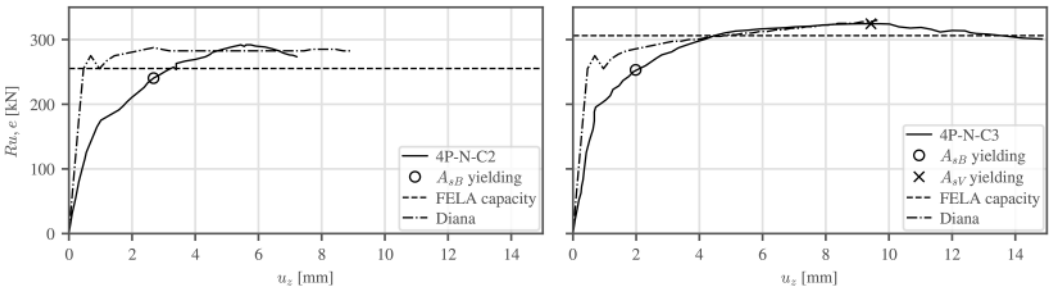

Figure 8. Load-displacement plot for the two specimens. Note that the y-axis shows the load in one pile only.

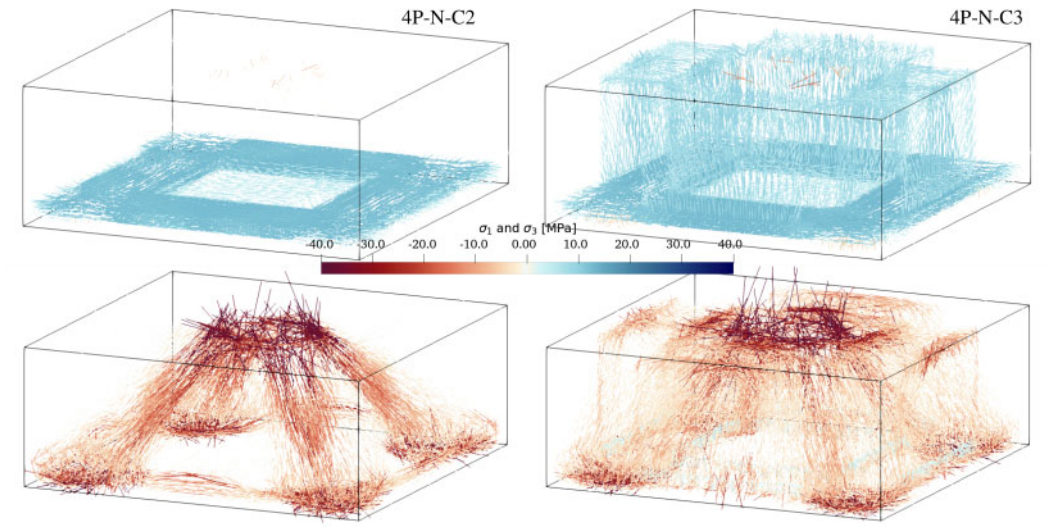

Figure 9. Principal stress flow predicted from by the FELA models for the two specimens. Bottom: Third principal stress, top: first principal stress.

Contrary to the NLFEA calculation, FELA calculations do not give any information about the load-displacement behavior of the model. Instead, the presence of sufficient ductility is a requirement for the safe use of the method. In the present case, even with a brittle failure of specimen 4P-N-C2, the capacities found from FELA are found to be safe.

For both specimens, the capacity found from the FELA calculations is lower than the ultimate load. However, they are in both cases larger than the load, which gives yielding of the bunched reinforcement A_{sB}. From this observation, we can conclude that the FELA calculations can utilize at least some of the reinforcement between the piles. Also, the inclusion of the shear reinforcement makes the FELA model better able to utilize this reinforcement, which can be seen from the larger difference between the yielding of bunched reinforcement and the FELA capacity for specimen 4P-C2-N3 compared to specimen 4P-C2-N2. In other words, the presence of the shear reinforcement allows for new load-paths. Consequently, the capacity is about 200 kN higher when the shear reinforcement is introduced, which is 20% higher than without shear reinforcement. The DIANA FEA calculations are able to very accurately determine the ultimate loads for both specimens. One of the reasons for the accurate calculation, and difference from the FELA model, is that hardening is included in the NLFEA model so the ultimate capacity of the reinforcement can be reached. From 2, it is seen that the ultimate strength of the reinforcement is in average 17% higher than the yield strength.

4.4.2 Stress flow

Figure 9 shows the stress flow found from the FELA calculations by plotting the first and third principal stress vectors of the two specimens. The stress flow for specimen 4P-C-N2 is entirely predictable with a strut originating at each pile and terminating at the column, utilizing the bunched reinforcement and, to a lesser degree, the reinforcement between the piles to carry the tie forces. The stress flow plot is clear and looks similar to a strut-and-tie model. The stress flow for specimen 4P-C-N3 is a bit more complicated since,

besides the main strut action, secondary load paths are also present utilizing the shear reinforcement between the piles. For both specimens, it can be seen that the struts terminate on the very edge of the column, which makes sense since this will give the most direct transfer of compression from the piles to the column.

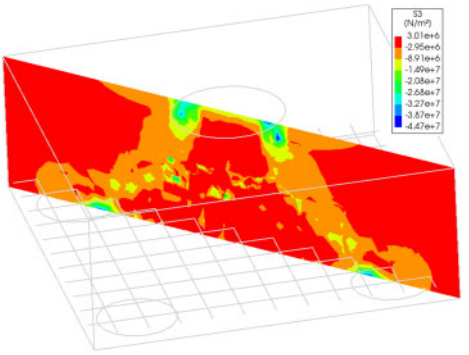

Figure 10. Third principal stress plot for the Diana model of specimen 4P-N-C2 at peak load.

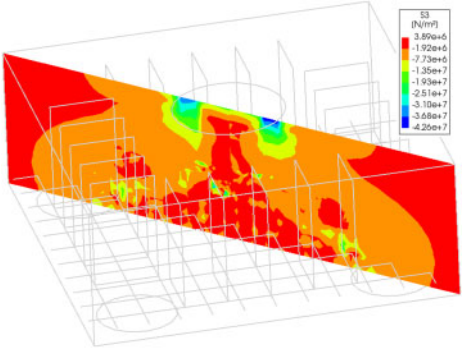

Figure 11. Third principal stress plot for the Diana model of specimen 4P-N-C3 at peak load.

4.4.3 Deformation and collapse mode

The flow of compression at the peak load in the DIANA FEA model can be seen in Figure 10 for specimen 4P-N-C2 and in Figure 11 for specimen 4P-N-C3. The figures show surface plots through the diagonal. The results are quite similar to the FELA results, with a concentrated strut from the pile towards the edge of the column for 4P-N-C2, and a more complicated load path for 4P-N-C3. In both cases the load transferred at the edge of the column, which is also similar to the FELA calculations.

The NLFEA model, which uses a deformation-based model, can show the deformation state at any point in the load history. This is not the case for FELA, which has no information about the deformation due to the rigid-plastic material model. However, the dual variables of the stress equilibrium (4b) can be interpreted as a collapse mode. The collapse mode shows how each part of the model will move with respect to each other at collapse but says nothing about the magnitude of the deformations.

A plot of the collapse mode from the FELA calculations for the two specimens can be seen in Figure 12, and a deformation plot at peak load for the NLFEA calculations can be seen in Figure 13.

Specimen 4P-N-C2 shows a localized collapse with the piles moving upwards. This collapse seems consistent with a punching failure after yielding of the bunched reinforcement, as reported by the experiment. The deformation plot from the NLFEA calculations also shows a localized failure indicative of the aforementioned punching failure mode.

Specimen 4P-N-C3 was reported to have a flexural failure in the experiments, and this also seems consistent with the FELA collapse mode, and the NLFEA deformation plot.

Even if the FELA calculations yield no information about the load-displacement behavior, in this case, the collapse mode still reveals something since a punching failure would generally be assumed to be less ductile than a flexural one.

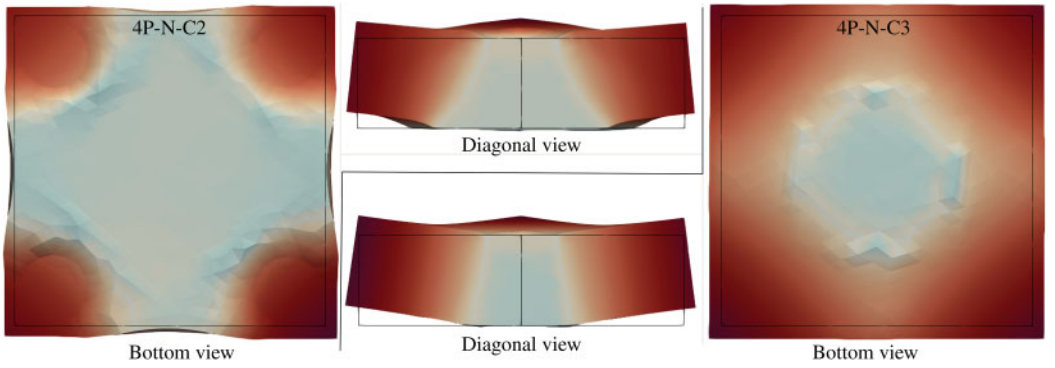

Figure 12. Collapse mode predicted from by the FELA models for the two specimens. The coloring of the faces is the relative vertical displacement.

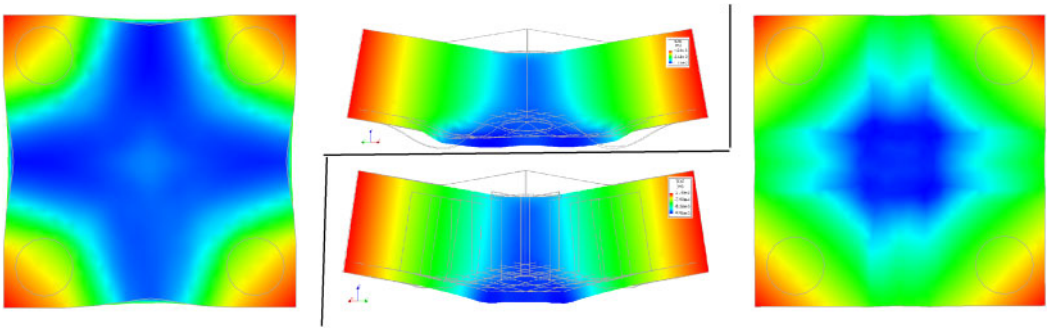

Figure 13. Collapse mode predicted from by the NLFEA models for the two specimens.

5 CONCLUSION

Computational models of two four-pile cap experiments using Finite Element Limit Analysis (FELA) and the Non-Linear Finite Element Method (NLFEM) software DIANA FEA have been presented. Results obtained from the two models have been compared to each other and the experimental findings from the literature. Both models were able to determine the capacity to a satisfactory degree and foresee the mode of collapse. The load-displacement plot obtained from the DIANA FEA model showed good agreement with the experimental results.

While DIANA FEA, and NLFEM in general, can describe the behavior of a structure very accurately, the precision also comes at the cost of increased complexity. On the other hand, FELA can only give information about the ultimate limit state. However, the model is also simpler. The simplicity can mean faster modeling time and calculation time, but the structures must be ductile to use FELA safely. In conclusion, both methods have their strengths and weaknesses, and it is essential to be mindful of these and use the right tool for a given task. Furthermore, the two methods can be used as independent model control for each other.

REFERENCES

Anderheggen, E. & H. Knöpfel (1972, dec). Finite element limit analysis using linear programming. *International Journal of Solids and Structures 8*(12), 1413–1431.

Andersen, M. E. M., P. N. Poulsen, & J. F. Olesen (2021, may). Finite-Element Limit Analysis for Solid Modeling of Reinforced Concrete. *ASCE Journal of Structural Engineering 147*(5), 04021051.

Andersen, M. E. M., P. N. Poulsen, & J. F. Olesen (2022, jan). Partially mixed lower bound constant stress tetrahedral element for Finite Element Limit Analysis. *Computers & Structures 258*, 106672.

Bisbos, C. D. & P. M. Pardalos (2007, aug). Second-Order Cone and Semidefinite Representations of Material Failure Criteria. *Journal of Optimization Theory and Applications 134*(2), 275–301.

Boyd, S. & L. Vandenberghe (2004). *Convex optimization* (1 ed.). New York: Cambridge University Press.

DIANA, F. E. A. (2017). Diana User's Manual, Release 10.2.

Drucker, D. C., W. Prager, & H. J. Greenberg (1952). Extended limit design theorems for continuous media. *Quarterly of Applied Mathematics 9*(4), 381–389.

Feenstra, P. H. (1993). *Computational aspects of biaxial stress in plain and reinforced concrete*. Ph. D. thesis, Delft University of Technology.

Fib (2013, oct). *fib Model Code for Concrete Structures 2010*. Weinheim, Germany: Wiley-VCH Verlag GmbH & Co. KGaA.

Gvozdev, A. (1960). The determination of the value of the collapse load for statically indeterminate systems undergoing plastic deformation. *International Journal of Mechanical Sciences 1*(4), 322–335.

Hendriks, M. A. N., A. de Boer, & B. Belletti (2017). Guidelines for nonlinear finite element analysis of concrete structures. Technical report, Rijkswaterstaat Technisch Document (RTD), Rijkswaterstaat Centre for Infrastructure, RTD.

Herfelt, M. A. (2017). *Numerical limit analysis of precast concrete structures - A framework for efficient design and analysis*. Ph.d. thesis, Technical University of Denmark (DTU), Kgs. Lyngby.

Herfelt, M. A., J. Krabbenhøft, & K. Krabbenhøft (2019). Practical Design and Modelling of Precast Concrete Structures. *Current Trends in Civil and Structural Engineering 3*(2), 8–11.

Jensen, T. W., P. N. Poulsen, & L. C. Hoang (2018, nov). Finite element limit analysis of slabs including limitations on shear forces. *Engineering Structures 174*, 896–905.

Krabbenhøft, K., A. V. Lyamin, & S. W. Sloan (2008). Three-dimensional Mohr-Coulomb limit analysis using semidefinite programming. *Communications in Numerical Methods in Engineering 24*(11), 1107–1119.

Larsen, K. P. (2010). *Numerical Limit Analysis of Reinforced Concrete Structures: Computational Modeling with Finite Elements for Lower Bound Limit Analysis of Reinforced Concrete Structures*. Ph.d. thesis, Technical University of Denmark (DTU), Kgs. Lyngby.

Lertsrisakulrat, T., K. Watanabe, M. Matsuo, & J. Niwa (2001). Experimental study on parameters in localization of concrete subjected to compression. *Doboku Gakkai Ronbunshu 2001*(669), 309–321.

Martin, C. M. & A. Makrodimopoulos (2008). Finite-Element Limit Analysis of Mohr–Coulomb Materials in 3D Using Semidefinite Programming. *Journal of Engineering Mechanics 134*(4), 339–347.